Journal of ELECTRONIC MATERIALS, Vol. 36, No. 8, 2007
DOI: 10.1007/s11664-007-0159-8

Special Issue Paper

Comparative Study of HgCdTe Etchants: An Electrical Characterization

SHUBHRANGSHU MALLICK,[1,4] RAJNI KIRAN,[2] SIDDHARTHA GHOSH,[1] SILVIU VELICU,[3] and SIVALINGAM SIVANANTHAN[2]

1.—Photonics and Spintronics Laboratory, University of Illinois at Chicago, 851 S. Morgan St., Chicago, IL 60607, USA. 2.—Microphysics Laboratory, University of Illinois at Chicago, 845 W. Taylor St., Chicago, IL 60607-7059, USA. 3.—590 Territorial Drive, Unit B, Bolingbrook, IL 60440, USA. 4.—e-mail: smalli1@uic.edu

A comparative study of wet etchants for both molecular beam epitaxy (MBE) and liquid phase epitaxy (LPE) grown *n*- and *p*-type samples was performed using capacitance–voltage (C–V) characteristics and surface recombination velocity (SRV) extracted from photoconductive decay (PCD) measurements. Different wet etchants were divided in two categories, (i) where bromine is a direct reagent in the etching solution and (ii) where bromine is a byproduct after reaction among different reagents. Negative shift of the flat-band voltages were observed for both *n*- and *p*-type samples treated with second category of etchants. A decrease in minority carrier lifetimes and an increase in the surface recombination velocities were also observed for the *n*-type samples treated with second category of etchants.

Key words: ZnS, CdTe, stacked passivation, minority carrier lifetime, capacitance–voltage characteristics, surface recombination velocity

INTRODUCTION

$Hg_{1-x}CdxTe$ (MCT; $x \equiv$ Cd composition) infrared detectors offer the possibility to tune the material cut-off wavelength between 1 μm and 14 μm in order to adapt the detector detection waveband to the application need. With proper theoretical designs different types of emitters and detectors have been studied and many of them have been fabricated.[1–5] During the last few years, there has been tremendous research effort devoted to various aspects of surface treatments, which results in evolution of new surface treatments along the years.[6,7] While sophisticated focal plane arrays of sizes as large as $1{,}024 \times 1{,}024$ and more are now well under the manufacturing phase, there remain many unanswered questions about the nature of HgCdTe surface, answers to which would improve the performance, yield and stability of the focal plane arrays.

Most of the HgCdTe devices are processed by wet etching technique. As etching is a surface treatment, different etchants would lead to different surface conditions. In wider bandgap material, it is quite reasonable to ignore these changes but in narrow bandgap material such as HgCdTe, these surface changes could make a significant difference and this in turn could affect the device performance. Therefore, it is quite necessary to study the effect of etchants on the HgCdTe surface, an effort that has been made here.

Passivation has been helpful especially for these narrow bandgap materials to minimize the effects from the surface states by saturating them. In HgCdTe, ZnS and CdTe or a stack of both has been established as potential candidates for passivants,[8–10] and there have been a few studies which have dealt with comparisons among these passivants.[11] However, the surfaces are needed to be freshly etched and properly treated before passivation, which helps passivant molecules to search for the lowest energy surfaces resulting in a superior

(Received October 16, 2006; accepted March 21, 2007; published online July 18, 2007)

quality passivation film. As surface gets affected differently for different etchants, that can also affect the passivation quality and hence the device characteristics.

In our study, we have focused on a comparative study among different wet etchants in HgCdTe technology. Capacitance–voltage (C–V) characteristics were measured and surface recombination velocities (SRV) were extracted from photoconductive decay measurements (PCD) on both liquid phase epitaxy (LPE) and molecular beam epitaxy (MBE) grown samples to characterize the surface after treatment with different etchants.

WET ETCHING IN HgCdTe

HgCdTe is a ternary alloy, composed of two II–VI compounds HgTe and CdTe. From the previous literature it becomes evident that both of these compounds get etched away in the acidic solution.[12,13]. The change in the free energy (ΔF) during etching is the driving force for any etching reaction, which determines the rate of etching. The lower the value of ΔF, the higher is the etching rate.

$$\mathrm{CdTe} + 2\mathrm{h}^{+} \rightarrow \mathrm{Cd}^{+2} + \mathrm{Te}^{0}; \quad \Delta F = 3.5\,\mathrm{kcal/mol}$$

$$\mathrm{CdTe} + 6\mathrm{h}^{+} \rightarrow \mathrm{Cd}^{+2} + \mathrm{Te}^{+4}; \quad \Delta F = 55.8\,\mathrm{kcal/mol}$$

$$\mathrm{HgTe} + 2\mathrm{h}^{+} \rightarrow \mathrm{Hg}^{+2} + \mathrm{Te}^{0}; \quad \Delta F = 46\,\mathrm{kcal/mol}$$

$$\mathrm{HgTe} + 6\mathrm{h}^{+} \rightarrow \mathrm{Hg}^{+2} + \mathrm{Te}^{+4}; \quad \Delta F = 98.5\,\mathrm{kcal/mol}$$

It becomes clear from the energy data table that to etch one mole of CdTe,[13] it is required to have a minimum ΔF of 3.5 kcal, while for HgTe the corresponding number is 46 kcal.[13] As a result, although HgTe bond is much weaker than CdTe, CdTe becomes more unstable in etching solution resulting in a faster etching rate.[12,13] This is the basis of all HgCdTe wet etching.

CATEGORIES OF WET ETCHANTS

In our comparative study, we have divided different wet etchants in two categories. In the first one, bromine was considered to be a direct reagent, and in the second one, bromine is emerged as a byproduct of a reaction among different reagents. Bromine–methanol (Br–MeOH), bromine lactic acid, bromine ethylene glycol etc. are considered as the examples of the first category of etchants and a mixture of deionized (DI) water, hydrobromic acid (HBr), and hydrogen peroxide (H_2O_2) or a mixture of ethylene glycol, HBr and H_2O_2 etc. are the representatives of the second category etchants. In the first category, Br_2 is reduced by losing two holes and is converted to Br^{-}, and the Te^{-2} is oxidized by accepting those two holes and is converted to Te^{0}. In the following steps, Br^{-} dissolves the Cd^{+2} or Hg^{+2} cations to form $CdBr_2$ and $HgBr_2$[12] respectively.

$$\mathrm{Br}_2 \rightarrow 2\mathrm{Br}^{-} + 2\mathrm{h}$$

$$\mathrm{Te}^{-2} + 2\mathrm{h} \rightarrow \mathrm{Te}^{0}$$

But in the second category, Br_2 is not directly available in the etching solution and emerges as a reaction between HBr and H_2O_2 solution. Once Br_2 is available in the solution, HgCdTe is etched by a similar procedure. But unlike the first category of etchants, a reversible hydrolysis reaction occurs between these two byproducts because of the simultaneous presence of Br_2 and water in the same solution. This results in the formation of HBr and its oxide counter (HBrO). HBrO reacts again with Te^{-2} to leave an excess of tellurium dioxide (TeO_2), HBr and an excess of two electrons.[12,13]

$$\begin{aligned} &2\mathrm{HBr} + \mathrm{H_2O_2} \rightarrow \mathrm{Br_2} + 2\mathrm{H_2O} \\ &\mathrm{Br_2} + \mathrm{H_2O} \rightarrow \mathrm{HBr} + \mathrm{HBrO} \\ &2\mathrm{HBrO} + \mathrm{Te}^{-2} \rightarrow \mathrm{TeO_2} + 2\mathrm{HBr} + 2\mathrm{e} \end{aligned} \quad (1)$$

EXPERIMENT

Samples studied in these experiments were grown both by LPE as well as MBE. The details of the compositional structures of these samples are given in Fig. 1a–d, respectively. The samples were thoroughly cleaned in warm (40°C) acetone, warm

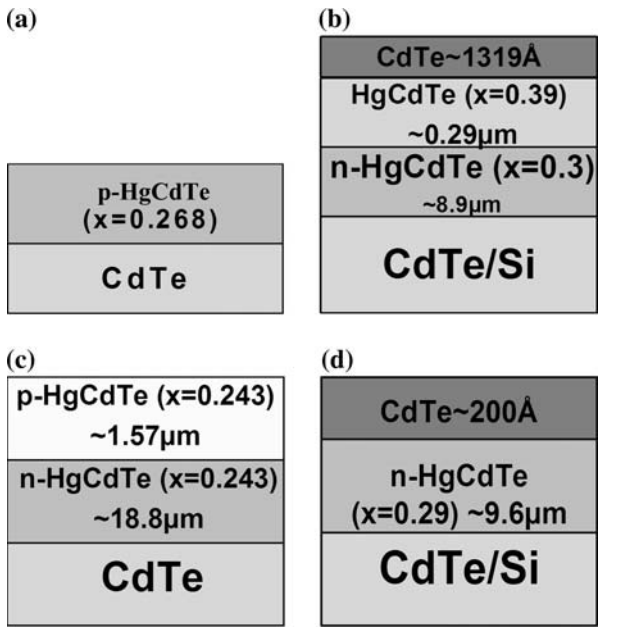

Fig. 1. Structural schematic diagram of samples (a) MWIR sample HCT 950322 (x = 0.268), (b) MWIR sample HCT 2228 (x = 0.3), (c) MWIR HCT 639 (x = 0.23), and (d) HCT 2412 (x = 0.29).

methanol and DI water, each for 5 min. Then they were dried with dry N_2 purge before treating them with respective etchants. After etching, samples were rinsed in the respective solvents and DI water for 5 min each and subsequently purged again with dry N_2 to remove any water droplet before loading it for ZnS passivation. While etching the samples, careful attention was paid in order to etch the same thickness of different pieces from the same wafer. This was strictly followed to avoid any effect of variation of thickness for different samples treated with different etchants. Most of the samples had a top or a cap or both layers, so during etching it was ensured to etch through both the top and the cap layers.

The ZnS passivation was done by electron beam (e-beam) evaporation technique using a Thermionics chamber. The samples were loaded upside down at room temperature. The chamber was pumped down till the pressure reached $1–2 \times 10^{-6}$ torr. The evaporation started with a slow and controlled deposition rate of less than 0.5 Å/s till 1,000 Å. The e-beam was kept below 5 mA during this time. Afterwards the deposition rate was ramped to 1–1.2 Å/s untill 4,000 Å and correspondingly the e-beam current was increased to 6.5–7 mA.

After passivation, the C–V samples are photoshaped for making metal contact on active HgCdTe layer and on the passivation layer. The metal deposition rate was also kept around 1 Å/s to avoid any damage of the active layer or the passivation layer during deposition. Gate metals were circular in shape with a diameter around 300 μm. C–V characteristics were also performed to verify the insulating property of the passivation layer (Fig. 2a). This was carried out also to ensure that the metal-semiconductor is ohmic where as the metal-passivation contact is Schottky. A cross-section of the C–V sample is shown in Fig. 2b.

In order to conduct the comparative study among different etchants, C–V analysis was performed and PCD measurements were taken. In PCD measurements, the sample was excited with a pulsed AlGaAs laser ($\lambda_c = 905$ nm) to generate excess minority carriers leading to a conductivity change. The bulk lifetime and the surface recombination parameters were extracted from the decay curves and were plotted as a function of temperature. All the C–V measurements were performed at 77 K temperature and 1 MHz frequency. The voltage was swept with the help of an Agilent 4156B Semiconductor Measurement Unit and the corresponding capacitances were stored with the help of an HP 4275A LCR Meter. The C–V and PCD measurement set-up is shown in Fig. 3a and b.The flat-band voltage of the C–V data for both *n*- and *p*-type samples were defined as the voltage where depletion region starts forming in the forward sweep of the voltage. No additional surface treatment was performed to reduce the hysteresis of the C–V data. This was avoided seeing the effect of the etchants only on the C–V graphs.

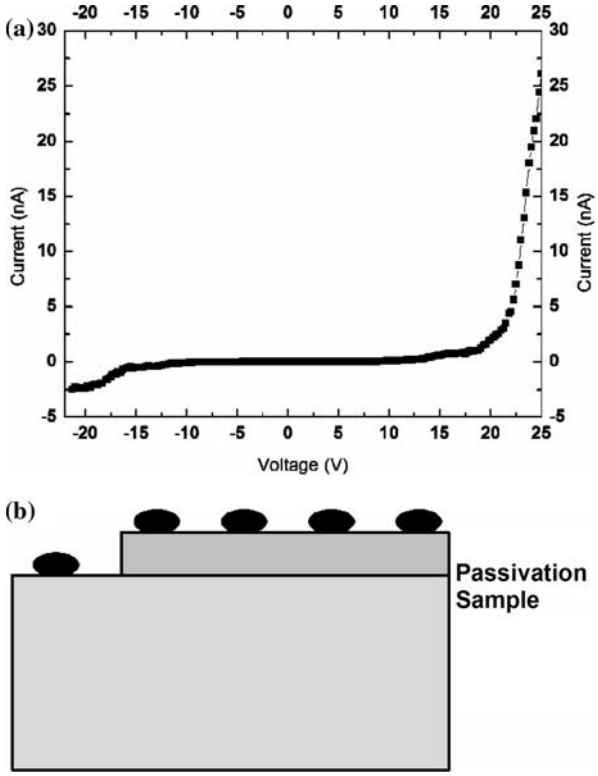

Fig. 2. (a) Current–voltage characteristics of the ZnS passivated HgCdTe layer. (b) Cross-section of the C–V sample.

RESULTS AND DISCUSSIONS

Etching is a surface treatment, so it affects the surface properties rather than bulk properties. Because of this, the comparative study among different etchants was carried out with the help of C–V analysis and SRV extracted from minority carrier lifetime, which gave a direct insight of the surface. For this narrow bandgap material, surface plays a dominant role, especially at low temperatures when the Auger mechanism is insignificant and the carrier concentration is controlled by doping. So all the C–V measurements were carried out at 77 K and all the SRVs were extracted from the change in conductivities at 78 K. If any active surface state was introduced during the respective etching treatments, C–V analysis would result in a relative shift of the flat band voltage, provided passivation was carried at the same time. From the nature of the shift of the flat-band voltage, the polarity of the surface state was determined.

Two adjacent pieces from the same p-type LPE grown HCT950322 were selected for the first set of experiments. The first one was treated with 1% Br–MeOH for 30 s and the other one was treated with 50DI + 10HBr + $1H_2O_2$ for 18 s. The respective etching timings were calibrated to etch around 5,000 Å from the top. A negative shift of the flat-band voltage in case of 50DI + 10HBr + $1H_2O_2$ was observed while comparing the C–V data (Fig. 3).

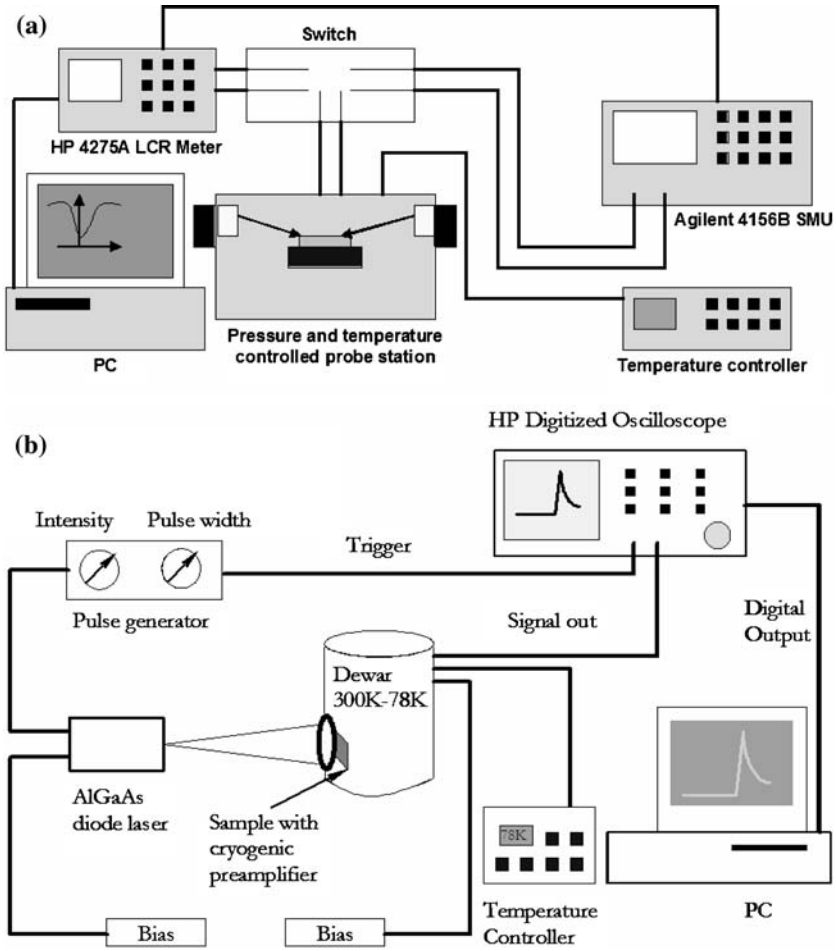

Fig. 3. Schematic of the (a) C–V setup and (b) PCD setup.

The flat-band voltage for 1%Br–MeOH treated sample was found at –0.7 V while for the other etchant it was observed at –4.5 V (Fig. 4). In the second set, the etching was performed for a little longer durations, 45 s for 1%Br–MeOH and 24 s for 50DI + 10HBr + $1H_2O_2$, on two other adjacent pieces from the same wafer. Approximately 8,000 Å of HgCdTe was removed from the top. An increase in the negative shift of the flat-band voltage was noticed this time (Fig. 5) for 50DI + 10HBr + $1H_2O_2$ treated sample. For 1%Br–MeOH treated sample the flat band voltage was at the same location but for 50DI + 10HBr + $1H_2O_2$ treated sample the flat band shifted to –6.5 V. Similar experiments were performed on *n*-type HCT2228 and for a short duration etch (30 s for 1%Br–MeOH and 18 s for 50DI + 10HBr + $1H_2O_2$). The flat-band voltages were at –2 V and –3 V, respectively (Fig. 6). For a relatively longer duration etch (45 s for 1% Br–MeOH and 24 s for 50DI + 10HBr + $1H_2O_2$), the flat-band voltage for 50DI + 10HBr + $1H_2O_2$ treated sample moved to –4 V, whereas for the 1% Br–MeOH treated sample the flat-band voltage remained at the same –2 V (Fig. 7). As discussed earlier, surface of DI + HBr + H_2O_2 treated sample becomes rich of trapped electrons due to the

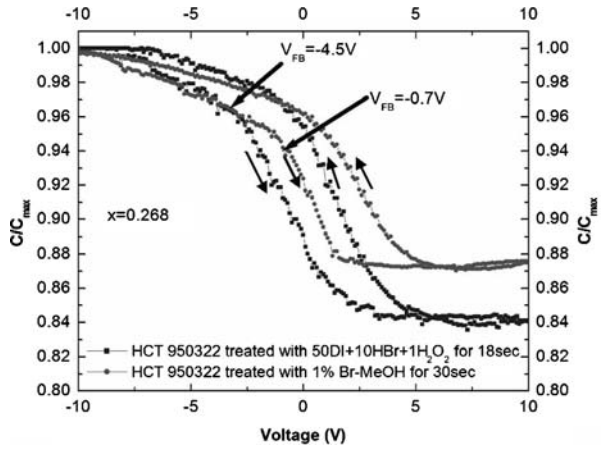

Fig. 4. C–V characteristics on HCT 950322 after 1% Br–MeOH treatment for 30 s (•) and 50DI + 10HBr + $1H_2O_2$ treatment for 18 s (■).

reversible hydrolysis reaction between water and Br_2 (Eq. 1). So in equilibrium, the band bends downward for both *p*-type and *n*-type samples, as shown in Fig. 8. As a consequence, an excess amount of negative voltage is applied at the gate in order to achieve a flat-band condition, which explains the

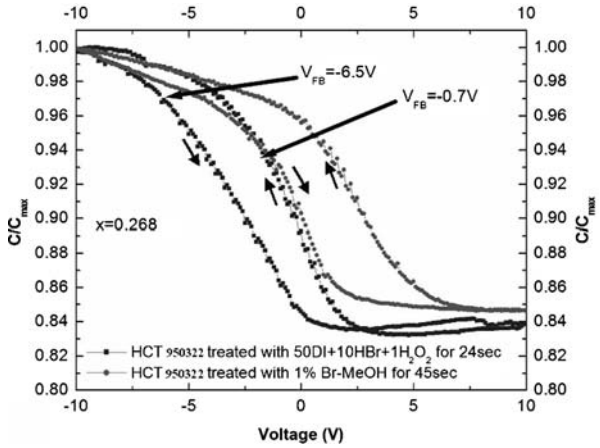

Fig. 5. C–V characteristics on HCT 950322 after 1% Br–MeOH treatment for 45 s (•) and 50DI + 10HBr + 1H_2O_2 treatment for 24 s (■).

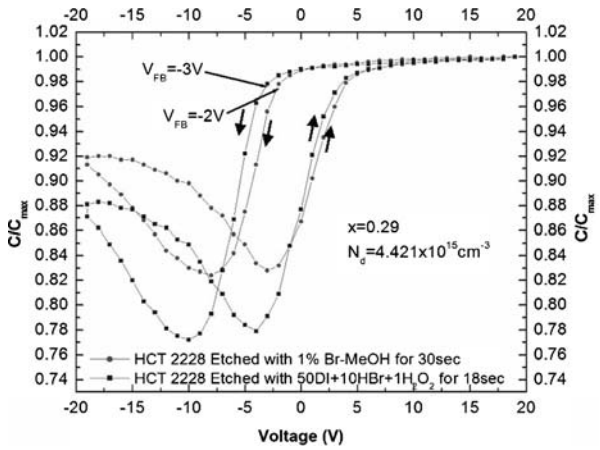

Fig. 6. C–V characteristics on HCT 2228 after 1% Br–MeOH treatment for 30 s (•) and 50DI + 10HBr + 1H_2O_2 treatment for 18 s (■).

negative-shift of the flat-band voltage for 50DI + 10HBr + 1H_2O_2 treated case. An increase in the etching time followed the increase in the concentration of trapped electrons resulting in an increase in the negative shift of the flat-band voltage.

The first set of PCD experiments was conducted on two adjacent pieces of an annealed LPE grown *n*-type sample HCT639. One of them was treated with 1% Br–MeOH for 2 min 30 s and the second one was treated with 50DI + 10HBr + 1H_2O_2 for 2 min to etch around 2 μm from the top. A comparison of minority carrier lifetimes as a function of 1000/T showed a decrease of minority carrier lifetime of 400 ns for 50DI + 10HBr + 1H_2O_2 treated sample in the low temperature range (Fig. 9). Surface recombination velocities were extracted from the data at 78 K using a similar procedure as discussed in our last work.[11] All the

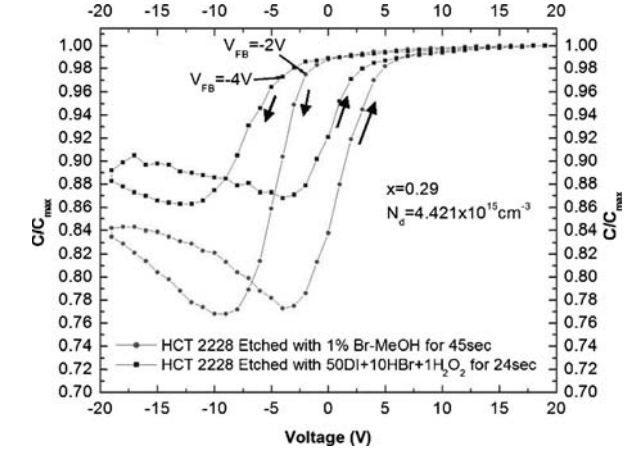

Fig. 7. C–V characteristics on HCT 2228 after 1% Br–MeOH treatment for 45 s (•) and 50DI + 10HBr + 1H_2O_2 treatment for 24 s (■).

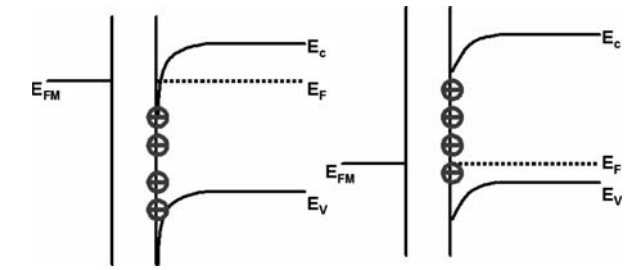

Fig. 8. Band bending for both *n*- and *p*-type sample, in both case the flat-band shifts in the negative direction.

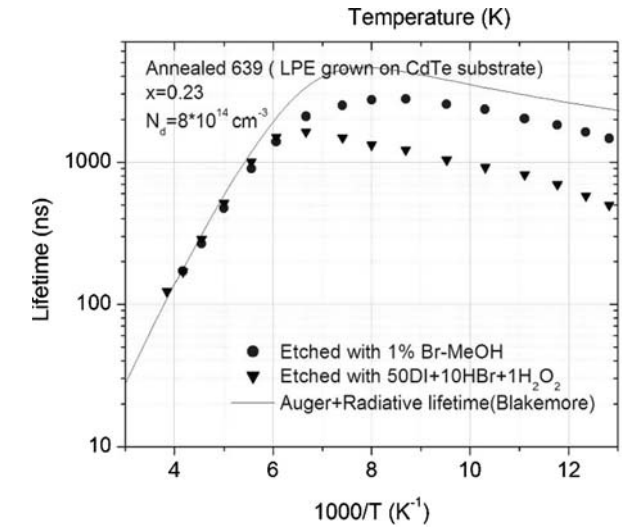

Fig. 9. Comparison of minority carrier lifetime of 50DI + 10HBr + 1H_2O_2 1% Br–MeOH treated HCT639 sample.

variables used in Eq. 2 are explained in details in Ref. 11. The data at 78 K were fitted with a scaled version of Eq. 2 using Matlab interface. The scaling factor was decided from the sample resistivity, geometry and the applied bias.

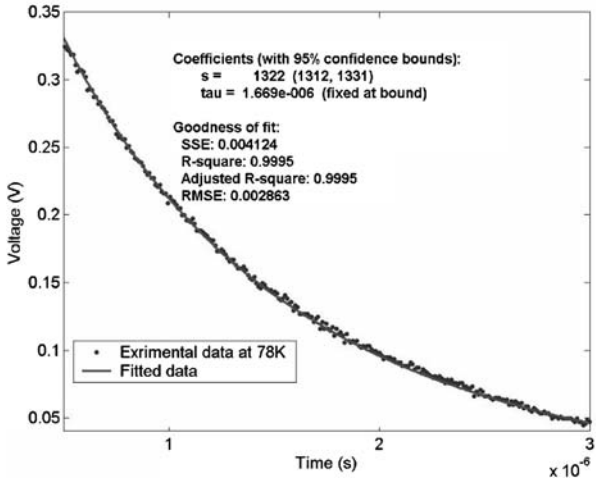

Fig. 10. Extraction of the surface recombination velocity for the 1% Br–MeOH treated LPE grown HCT639 sample.

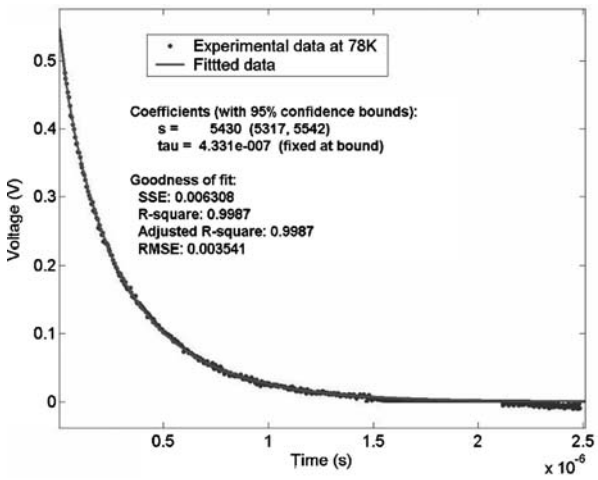

Fig. 11. Extraction of the surface recombination velocity for the 50DI + 10HBr + $1H_2O_2$ treated LPE grown HCT639 sample.

$$\Delta p(t) = \alpha I_0 e^{-\frac{t}{\tau}} \left[A e^{\alpha^2 Dt} Erfc(\alpha\sqrt{Dt}) + B e^{S^2 t/D} Erfc\left(S\sqrt{\frac{t}{D}}\right)\right] \quad (2)$$

The fitted data showed that for 1% Br-MeOH, the extracted surface recombination velocity was 1.3×10^3cm/s (Fig. 10) whereas for 50DI + 10HBr + $1H_2O_2$ the extracted surface recombination velocity was 5.43×10^3cm/s (Fig. 11). The effective minority carrier lifetime for the Br–MeOH treated sample at 78 K was 1699 nsec whereas for DI + HBr + H_2O_2 treated sample it was 433 ns. So an increase of the extracted surface recombination velocity by a factor of 5 and a decrease of minority carrier lifetime by a factor of 4 was observed in the 50DI + 10HBr + $1H_2O_2$ treated sample. Similar experiments were carried out for n-type MBE grown on CdTe/Si wafer HCT2412. The extracted surface recombination velocity in this case also showed similar behaviors. In the Br–MeOH treated sample at 78 K the extracted surface recombination velocity was 1.3×10^4 cm/s and the effective minority carrier lifetime was 942 ns (Fig. 12) and for DI + HBr + H_2O_2 treated sample, the corresponding values were 2.8×10^4 cm/s and 219 ns, respectively (Fig. 13). A decrease in the minority carrier lifetime by a factor of 4.5 and an increase of the surface recombination velocity by a factor of 2 was observed in case of DI + HBr + H_2O_2 treated sample. The PCD measurement data for both LPE and MBE grown sample is summarized in Table I. In PCD measurements, as the laser illumination was turned on for n-type sample, electron–hole pairs were created. The generated minority carrier holes recombine at these electrons trapped at the surface, which

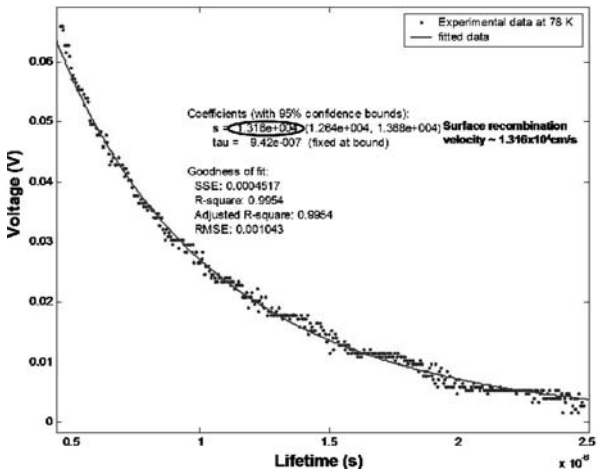

Fig. 12. Extraction of the surface recombination velocity for the 1% Br–MeOH treated MBE grown HCT2412 sample.

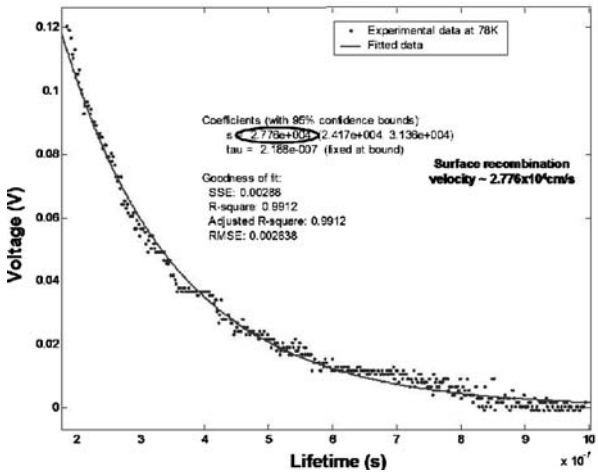

Fig. 13. Extraction of the surface recombination velocity for the 50DI + 10HBr + $1H_2O_2$ treated MBE grown HCT2412 sample.

Table I. Measured Data from PCD Experiment for HCT 639 and HCT 2412

At 78 K		Bromine-Methanol	DI + HBr + H_2O_2
HCT 639	Effective minority carrier lifetime (ns)	1,699	433
$x = 0.23$	Extracted surface recombination velocity (cm/s)	1.3×10^3	6.43×10^3
$N_a = 8 \times 10^{14}$ cm^{-3}			
HCT2412	Effective minority carrier lifetime (ns)	942	219
$x = 0.29$	Extracted surface recombination velocity (cm/s)	1.3×10^4	2.8×10^4
$N_d = 4.6 \times 10^{14}$ cm^{-3}			

reduces the effective minority carrier lifetime at low temperatures.

CONCLUSION

From both C–V analysis and SRV extracted from photoconductive decay technique, it was confirmed that a thin layer of negative charge was present in between the passivation and active layers for 50DI + 10HBr + $1H_2O_2$ treated samples. An increase in the etching time results in an increase of the flat-band voltage in the negative direction for 50DI + 10HBr + $1H_2O_2$ treated samples. An increase in minority carrier lifetime and correspondingly a decrease in SRV extracted from PCD measurements for both LPE and MBE grown *n*-type samples were observed for 1% Br_2–MeOH treated samples. In the near future, a more systematic comparative study among these etchants would be performed with the help of X-ray photoelectron spectroscopy.

ACKNOWLEDGEMENTS

This work is funded by Air Force Office of Scientific Research (AFOSR) under contract FA9550-06-C-0007 monitored by Dr. Donald Silversmith. We would like to thank BAE Systems and Fiqri Aqaridan from DRS Technologies for providing us some of the samples for this study.

REFERENCES

1. J. Bajaj, J.M. Arias, M. Zandian, J.G. Pasko, L.J. Kozlowski, R.E. DeWames, and W.E. Tennant, *J. Electron. Mater.* 24, 1061 (1995).
2. P. Mitra, S.L. Barnes, F.C. Case, M.B. Reine, P. O'Dette, R. Starr, A. Hairston, K. Kuhler, M.H. Weiler, and B.L. Musicant, *J. Electron. Mater.* 26, 482 (1997).
3. G. Destéfanis, A. Astier, J. Baylet, P. Castelein, J.P. Chamonal, E. DeBorniol, O. Gravand, F. Marion, J.L. Martin, A. Million, P. Rambaud, F. Rothan, and J.P. Zanatta, *J. Electron. Mater.* 32, 592 (2003).
4. S.M. Johnson, A.A. Buell, M.F. Vilela, J.M. Peterson, J.B. Varesi, M.D. Newton, G.M. Venzor, R.E. Bornfreund, W.A. Radford, E.P.G. Smith, J.P. Rosbeck, T.J. De Lyon, J.E. Jensen, and V. Nathan, *J. Electron. Mater.* 33, 526 (2004).
5. M. Walther, R. Rehm, F. Fuchs, J. Schmitz, J. Fleibner, W. Canaski, D. Eich, M. Finck, W. Rode, J. Wendler, R. Wollrab, and J. Ziegler, *J. Electron. Mater.* 34, 722 (2005).
6. M.Y. Lee, Y.S. Lee, and H.C. Lee, *J. Appl. Phys.* 44, L 1252 (2005).
7. S.H. Lee, H. Shin, H.C. Lee, and C.K. Kim, *J. Electron. Mater.* 26, 556 (1997).
8. Y.Nemirovsky and G.Bahir, *J. Vac. Sci. Technol. A* 7(2), 450 (1989).
9. Y. Nemirovsky , *J. Vac. Sci. Technol. A* 8(2), 1185 (1990).
10. O.P. Agnihotri, C.A. Musca, and L. Farone, *Semicond. Sci. Technol.* 13, 839 (1998).
11. R. Kiran, S. Mallick, S.R. Hahn, T.S. Lee, S. Ghosh, S. Sivanathan, and P.S. Wijewarnasuriya, *J. Electron. Mater.* 35, 1379 (2006).
12. V. Srivastav, R. Pal, B.L. Sharma, A. Naik, D.S. Rawal, V. Gopal, and H.P. Vyas, *J. Electron. Mater.* 34, 1440 (2005).
13. I.M. Kotina, L.M. Tukhkonen, G.V. Patsekina, A.V. Shchukarev, and G.M. Gusinkskii, *Semicond. Sci. Technol.* 13, 890 (1998).